Structural and Chemical Insights into Template-Free Nickel Oxide Nanopores: A Raman Spectroscopy Study

S. Virgin Jeba, S. Sonia, N. Annlin Bezy and *A. Lesly Fathima
Department of Physics, Holy Cross College (Autonomous), Nagercoil - 629004.
Affiliated to Manonmaniam Sundaranar University, Tirunelveli - 627012.
*Corresponding Author - Email: leslysat@gmail.com

ABSTRACT

Nanosized Nickel Oxide (NiO) has emerged as a versatile material with significant potential across various technological fields such as magnetic devices, catalysts, batteries, fuel cells and solar cells. Nickel Oxide (NiO) is a promising semiconductor material being used due to its variety of applications as many are dependent upon its typical shape. A simple and cost-effective hydrothermal method was used to synthesize NiO porous Nanostructures. The effect of pH on structure, morphology and RAMAN spectra of NiO porous nanostructures were investigated in detail. The present study reports a synthesis of nanoporous NiO by hydrothermal method characterized by XRD, SEM and RAMAN studies. The formation of pure and crystalline NiO nanostructures is confirmed by the XRD pattern. The nanoporous structure was confirmed from the FESEM analysis. The sample exhibited a uniform porous structure, with interconnected pores forming large channels throughout the material. The Raman spectra between 600 and 1500 cm^{-1} do not contain any other 1P, 2M magnon peaks is proof that NiO nanoparticles have transitioned from an antiferromagnetic state that was previously present in the sample. These findings are congruent with the conclusions that were reached from the XRD examination.

Keywords: *Hydrothermal method, Nickel Oxide, Porous, RAMAN*

1. Introduction

Over the past few decades, metal oxide nanoparticles have increasingly captured the interest of researchers due to their diverse and promising applications. Nickel Oxide (NiO), a prominent transition metal oxide, has been at the forefront of these investigations due to its wide band gap [1] and versatile functionalities [2]. They include catalysis [3], lithium-ion batteries [4, 5], smart windows [6], anti-ferro magnetic film [7], dye-sensitized photocathodes [8,9], thermal conductivity [10] and field emission studies [11]. There are many methods to synthesize NiO nanoparticles namely coprecipitation method, sonochemical method, solgel method combustion method, hydrothermal method. Among these, hydrothermal method is used as it is low cost, simple, effective and inexpensive with controlled sizes and morphological structure [12, 13]. In the present work Nickel Oxide porous nanostructures were synthesized

without any templates and the prepared samples were characterized by XRD, SEM and RAMAN.

2. Materials and Methods

2.1 Synthesis of nanoporous NiO nanostructures

In a typical NiO porous nanostructure synthesis process, 0.3 M of Nickel nitrate hexahydrate [$Ni(NO_3)_2$] was dissolved in 1:1 ratio of distilled water (DW) and ethanol, and stirred for 30 min in a magnetic stirrer. Also, 1 g of Tri sodium citrate ($Na_3C_6H_5O_7.2H_2O$) was dissolved in 1:1 ratio of DW and ethanol. The pH of this solution was adjusted to 14 using Tri ethyl amine and continuously stirred for 5 h to make a homogeneous mixture. This mixture was further transferred to Teflon lined stainless steel autoclave and hydrothermally treated at 180^{o}C for 12h and cooled down to room temperature naturally. The final precipitate obtained was washed several times with distilled water to remove the impurities and dried in hot air oven at 100^{o}C. The reactions were carried out by varying the pH value (i) pH = 8 (ii) pH = 10 (iii) pH = 12 (iv) pH = 14. The NiO porous nanostructures were optimized at pH = 14 in the reaction.

3. Results and Discussion

3.1 Structural analysis of nanoporous NiO

The XRD pattern of the as-prepared nanosized NiO porous nanostructure was shown in Fig 1. The formation of pure and crystalline NiO nanostructures is confirmed by the XRD pattern. The observed peaks are indexed at 2θ values corresponding to the crystallographic planes (222), (400), (440), (622), and (444), which align well with the standard data for NiO (JCPDS # 89-5881). All observed peaks are distinctly indexed to a pure face-centered cubic (FCC) structure, with no additional peaks corresponding to secondary phases or intermediate compounds, such as $Ni(OH)_2$ or Ni_2O_3. This confirms the purity of the products obtained after calcination.

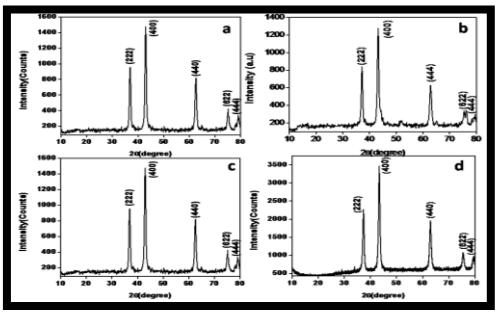

Fig. 1. XRD spectra of the synthesized NiO porous nanostructures by varying the pH value (i) pH = 8 (ii) pH = 10 (iii) pH = 12 (iv) pH = 14

3.2 FESEM analysis of NiO nanoporous structure

Fig. 2 shows the series of morphology prepared by varying the pH value. The optimized nanoporous structure was obtained at pH value of 14. At pH ~ 8, the structure was agglomerated and no porous was found. As the pH increased to 10, tiny pores began to form randomly on the surface. With further increases in pH to 12, both the number and diameter of the pores increased continuously. At pH 14, the sample exhibited a uniform porous structure, with interconnected pores forming large channels throughout the material.

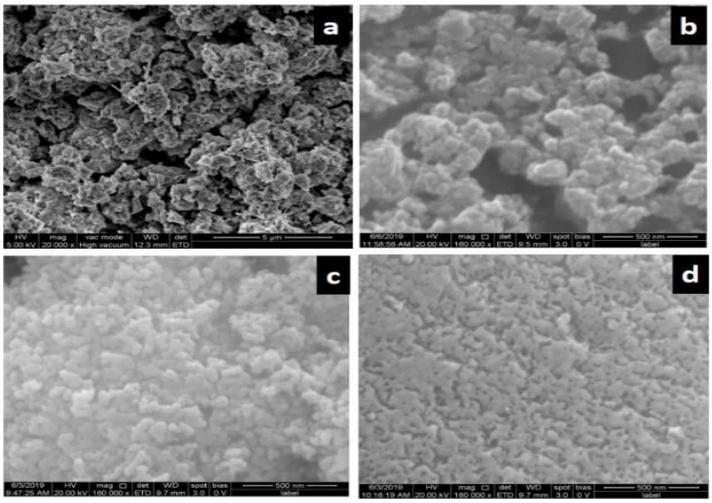

Fig. 2. FESEM images of NiO porous nanostructure prepared by varying the pH value (i) pH = 8 (ii) pH = 10 (iii) pH = 12 (iv) pH = 14

3.3 Raman analysis of NiO porous nanostructure

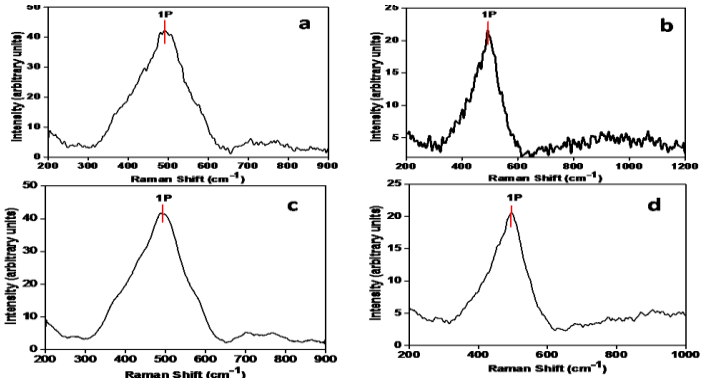

Fig. 3. Raman spectra of the synthesized NiO porous nanostructure by varying the pH value (i) pH = 8 (ii) pH = 10 (iii) pH = 12 (iv) pH = 14

Fig. 3 displays the Raman spectra of the synthesized NiO porous nanostructure by varying the pH value (a) pH = 8, (b) pH = 10, (c) pH = 12 and (d) pH = 14. These spectra were produced with a LABRAMHR Confocal Laser Micro Raman spectrometer at 514.5 nm and 250 mW. It is easy to see that the Raman spectrum has f peaks, and their relative heights are between 500 and 550 cm^{-1}. This is because of the powerful phonon–magnon interaction that

occurs on the particle surface. We were able to assign the peaks that occurred at 500-550 cm^{-1} corresponding to longitudinal optical (LO) phonon modes of NiO, respectively, by comparing them to the data that were anticipated for a cubic NiO single crystal. This allowed us to determine which modes correlate to the peaks. These modes are the fundamental contributors to the optical characteristics of NiO. The first-order Raman peaks that were discovered near to 520- 546 cm^{-1} (LO) must have been the result of parity-breaking faults because of this. Fig. 3 displays the Raman scattering spectra obtained from NiO porous nanostructure (a-d). Since first-order Raman scattering cannot occur in a face-centered cubic (FCC) structure, it is anticipated that the intensity of one-phonon scattering will dramatically rise in NiO (the band at less than 500 cm^{-1}) [14]. The Ni-O stretching mode is responsible for the vibrational peak that occurs at around 500 cm^{-1}. An increase in the intensity of the one-phonon mode Raman scattering peak reveals the imperfection of NiO nanostucture. This structural imperfection is due to the structural disorder caused by nickel interstitial, surface effects, and oxygen vacancies. According to the findings of this study, the intensity of the one-phonon band for the nanocrystalline form of NiO appears to be lower. On the other hand, we found that the intensity of the one-phonon band significantly increased when the NiO nanoparticles in question were smaller [15]. This result is supported by the increase in first-order Raman scattering observed in NiO, particularly in regions with significant concentrations of nickel vacancies. The enhanced intensity of the one-phonon band at 500 cm^{-1} is attributed to the increased surface-to-bulk ratio and higher defect concentration. Additionally, it was predicted that the frequency of the longitudinal optical (LO) mode would increase, leading to a downward adjustment in the frequency of all combination peaks. This helps to explain why this occurred. The fact that the Raman spectra between 600 and 1500 cm^{-1} do not contain any other 1P, 2M magnon peaks is proof that NiO nanoparticles have transitioned from an antiferromagnetic state that was previously present in the sample. These findings are congruent with the conclusions that were reached from the XRD examination, and they provide some insight into the overall quality of the crystal.

4. Conclusion

In summary we prepared NiO porous nanostructures with four different pH value without any template by hydrothermal method. The nanoparticles were characterized by XRD, SEM and RAMAN studies. The formation of pure and crystalline NiO nanostructure is confirmed by XRD pattern and the peaks observed were indexed. The optimized nanoporous structure was obtained at pH value of 14 and was confirmed by FESEM analysis. The fact that the Raman spectra between 600 and 1500 cm^{-1} do not contain any other 1P, 2M magnon peaks is proof

that NiO nanoparticles have transitioned from an antiferromagnetic state that was previously present in the sample. The findings from Raman spectra of the synthesized NiO porous nanostructure are congruent with the conclusions that were reached from the XRD examination, and they provide some insight into the overall quality of the crystal.

References

1. Reinert F., Steiner P., Hufner H., Schimtt J., Fink J., Knupper M., Sandal P., Bertel E. Synthesis and Characterization of NiO Nanoparticles by Thermal Decomposition Method, Z. Phys. 1995; B97: 83 - 93.
2. Anandan K., Rajendran V. Effect of Various Solvent on the Synthesis of NiO Nanopowders by Simple Sol-Gel Methods and Its Characterization, Nanosci. Nanotechnol. Int. J. 2012; 2: 24 - 29.
3. Berchmans S., Gomathi H., Rao G P. Electrochemical Enhancement of Nickel oxide Dispersed Graphene Sheets as Electrode Material for Energy Storage Application, J. Electroanal. Chem. 1995; 394: 267 - 270.
4. Poizot P., Laruelle S., Grugeon S., Dupont L., Tarascon J M. Nano-Sized Transition-Metal Oxides as Negative-Electrode Materials for Lithium-Ion Batteries, Nature 2000; 407: 496 - 499.
5. Reddy M.V., Subba Rao V., Chowdari B.V.R. LiVP2O7/C: A New Insertion Anode Material for High-Rate Lithium-Ion Battery Applications, Chem. Rev. 2013; 113: 5364 - 5457.
6. Granqvist C G. Handbook of Inorganic Electrochromic Materials Ed. Elsevier, Amsterdam, 1995.
7. Loudon J C. Antiferromagnetism in NiO Observed by Transmission Electron Diffraction. Phy. Rev. Lett. 2012; 109: 267404 - 267408.
8. He J., Lindstrom H, Hagfeldt A, Lindquist S E. Solid-state p-type dye-sensitized solar cells: progress, potential applications and challenges, J. Phys. Chem 1999; B103: 8940 – 8943.
9. Ji Z., Natu G., Wu. P-type e sensitize solar cells: An overview of factors limiting efficiency, ACS Appl. Mater. Interfaces 2013; 5: 8641 - 8648.
10. Sahoo P., Misra D., Chaubey G.S., Salvadaor J., Takas N.J., Poudeu P.F.P. Synthesis and characterization of NiO nanoparticles by thermal decomposition method, MRS Proc. 2010; 1256.
11. Varghese B., Reddy M.V., Yanwu Z., Lit C.S., Hoong T.C., Subba Rao G., Chowdari B.V.R., Wee A.T.S., Lim C.T., Sow C.H. Fabrication of NiO nanowall electrodes for high performance lithium-ion battery Chem. Mater 2008; 20: 3360 - 3367.

12. Ji Z., Natu G., Wu Y. Dye-sensitized solar cells strike back, ACS Appl. Mater. Interfaces 2013; 5: 8641 - 8648.
13. Nitin C., Sunayana S., Sharma M K., Chaturvedi R K. Detailed electrochemical probing of the pH dependent Redox behaviour of 1-methoxyphenazine. Int. J. Res. Chem. Environ. 2011; 1: 66 - 70.
14. Jiang D., Optical properties of NiO thin films fabricated by electron beam evaporation' Vacuum, 2012; 86: 1083 - 1086.
15. Wruck D., Rubin M. Electronic properties of electrochromic NiO films, Journal of the Electrochemical Society. 1993; 140: 1097.